J|A|C|S
ARTICLES
Published on Web 06/06/2002

Open-Framework and Microporous Vanadium Silicates

Xiqu Wang, Lumei Liu, and Allan J. Jacobson*

Contribution from the Department of Chemistry, University of Houston, Houston, Texas 77204-5003

Received March 8, 2002

Abstract: A series of novel vanadium silicates with open-framework and microporous structures has been synthesized under mild hydrothermal conditions. Ten distinct framework types have been identified that all have structures based on cross-linking single silicate sheets with square pyramidal $V^{IV}O_5$ units to give compounds with the general formula $A_r[(VO)_s(Si_2O_5)_p(SiO_2)_q]\cdot tH_2O$, where A is Na, K, Rb, Cs, or a combination. The vanadosilicate (VSH-*n*) structures have free channel diameters up to 6.5 Å and show good thermal stability, absorption, and ion-exchange properties, suggesting their potential for technological applications as molecular sieves or in catalysis.

Introduction

Porous crystalline materials that contain cavities and channels with dimensions on the nanometer scale have a wide range of important applications in molecular separations, as ion-exchangers, and in heterogeneous catalysis. The aluminosilicates or zeolites that have structures based on frameworks of connected tetrahedral SiO_4 and AlO_4 building units are the most important class of porous crystals that have commercial applications.[1−4] The aluminophosphates, substituted aluminophosphates,[5,6] gallophosphates,[7−9] and zinc and cobalt phosphates[10,11] are other examples of "zeotypes" based on tetrahedral building units that have been discovered in the past two decades in the search for new selective catalysts.[12]

A second, though less explored, class of open-framework solids contains compounds with structures formed by linking tetrahedra with other types of metal-ion-centered polyhedra such as octahedra or square pyramids. The possibility of constructing porous solids from mixed polyhedra became widely recognized with the work on the titanium silicates at Engelhard[13,14] and on metal phosphates and tin silicates at Exxon Research in the late 1980s.[15−17] Since then, a large number of mixed polyhedral frameworks containing phosphate groups have been synthesized. In contrast, relatively few silicates and germanates have been reported, though these are expected to have better stability over a wider range of catalytic conditions. Rocha and Anderson recently reviewed the known examples of transition metal silicates with open frameworks.[18] Several phases, for example the titanosilicate $Na_2TiSi_5O_{13}\cdot xH_2O$ (ETS-10)[19−22] and the zirconium germanate $(C_4N_2H_{14})ZrGe_2O_6F_2\cdot H_2O$ (ASU-15)[23] have wide channel systems and substantial micropore volume.

We have recently focused on vanadium metal silicates because they are expected to show better thermal and hydrothermal stability than the corresponding phosphates. Vanadium-based catalysts are known to be effective for oxidation chemistry due to the accessibility of multiple oxidation states, and consequently the vanadosilicates are potentially interesting catalysts. In fact, the catalytic properties of several tetrahedral silicate frameworks, for example, MEL and MTW, containing small amounts of vanadium substituted for silicon (Si/V $\geq \sim$80), have been reported.[24−26] In contrast to the large family of vanadophosphates, only one synthetic large-pore vanadosilicate (AM-6, isostructural with ETS-10) is known that contains

* To whom correspondence should be addressed. E-mail: ajjacob@uh.edu.

(1) Breck, D. W. *Zeolite Molecular Sieves*; John Wiley & Sons: New York, 1974.
(2) Barrer, R. M. *Zeolites and Clay Minerals*; Academic Press: London, 1978.
(3) Bekkum, H. V.; Flanigen, E. M.; Jansen, J. C. *Introduction to Zeolite Science and Practice*; Elsevier: Amsterdam, 1991.
(4) Meier, W. M.; Olsen, D. H.; Baerlocher, C. *Atlas of Zeolite Structure Types*; Elsevier: London, 1996.
(5) Wilson, S. T.; Lok, B. M.; Messina, C. A.; Cannan, T. R.; Flanigen, E. M. *J. Am. Chem. Soc.* **1982**, *104*, 1146.
(6) Lok, B. M.; Messina, C. A.; Patton, R. L.; Gajek, R. T.; Cannan, T. R.; Flanigen, E. M. *J. Am. Chem. Soc.* **1984**, *106*, 6092.
(7) Estermann, M.; McCusker, L. B.; Baerlocher, C.; Merrouche, A.; Kessler, H. *Nature* **1991**, ***352***, 320.
(8) Parise, J. B. *Inorg. Chem.* **1985**, ***24***, 4312.
(9) Férey, G. *C. R. Acad. Sci. Ser. C* **1998**, *1*, 1.
(10) Feng, P.; Bu, X.; Stucky, G. D. *Nature* **1997**, *388*, 735.
(11) Chen, J.; Jones, R. H.; Natarajan, S.; Hursthouse, M. B.; Thomas, J. M. *Angew. Chem., Int. Ed. Engl.* **1994**, *33*, 639.
(12) For a recent review, see: Cheetham, A. K.; Férey, G.; Loiseau, T. *Angew. Chem., Int. Ed.* **1999**, *38*, 3268.
(13) Kuznicki, S. M. (Engelhard Corp.). Large-pored crystalline titanium molecular sieve zeolite. U.S. Patent 4,853,202, 1989.
(14) Kuznicki, S. M. (Engelhard Corp.). Preparation of small-pored crystalline titanium molecular sieve zeolites. U.S. Patent 4,938,939, 1990.
(15) Corcoran, E. J., Jr.; Vaughan, D. E. W. *Solid State Ionics* **1989**, *32/33*, 423.
(16) Haushalter, R. C.; Strohmaier, K. G.; Lai, F. W. *Science* **1989**, *246*, 1289.
(17) Corcoran, E. W., Jr. *Inorg. Chem.* **1990**, *29*, 158.
(18) Rocha, J.; Anderson, M. W. *Eur. J. Inorg. Chem.* **2000**, 801.
(19) Kuznicki, S. M.; Thrush, K. A.; Allen, F. M.; Levine, S. M.; Hamil, M. M.; Hayhurst, D. T.; Mansour, M. *Synth. Microporous Mater.* **1992**, *1*, 427.
(20) Anderson, M. W.; Terasaki, O.; Ohsuna, T.; Philippou, A.; MacKay, S. P.; Ferreira, A.; Rocha, J.; Lidin, S. *Nature* **1994**, *367*, 347.
(21) Wang, X.; Jacobson, A. J. *Chem. Commun.* **1999**, 973.
(22) Howe, R. F.; Krisnandi, Y. K. *Chem. Commun.* **2001**, 1588.
(23) Li, H.; Eddaoudi, M.; Plévert, J.; O'Keeffe, M.; Yaghi, O. M. *J. Am. Chem. Soc.* **2000**, *122*, 12409.
(24) Dzwigaj, S.; Matsuoka, M.; Anpo, M.; Che, M. *J. Phys. Chem. B* **2000,** *104*, 6012.
(25) Centi, G.; Perathoner, S.; Trifiro, F.; Aboukais, A.; Aissi, C. F.; Guelton, M. *J. Phys. Chem.* **1992**, *96*, 2617.
(26) Moudrakovski, I. L.; Sayari, A.; Ratcliffe, C. I.; Ripmeester, J. A.; Preston, K. F. *J. Phys. Chem.* **1994**, *98*, 10895.

10.1021/ja020354l CCC: $22.00

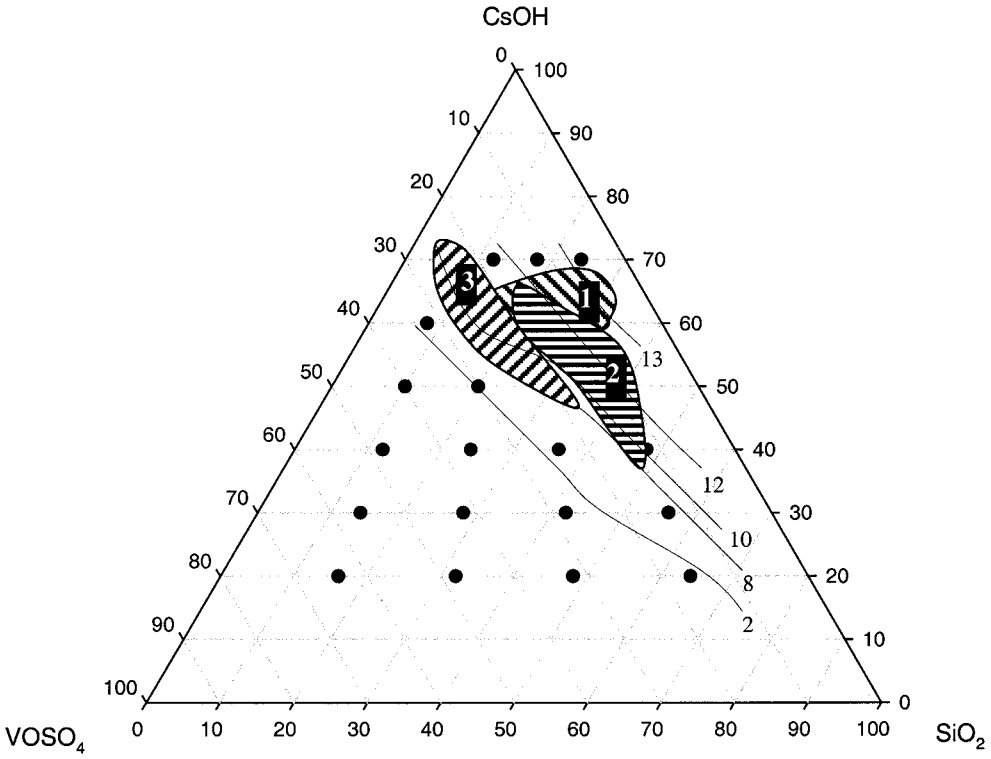

Figure 1. Composition triangle showing the regions of occurrence of compounds formed in the CsOH, SiO_2, $VOSO_4$ reaction system. 1, VSH-4Cs; 2, VSH-2Cs; 3, VSC-1 (cluster anion). Lines sketch compositions with equivalent final pH values; black dots are the initial survey compositions.

silicate tetrahedra in combination with oxovanadium(IV) species.[27] The only other known examples of open-framework vanadosilicates are the natural minerals cavansite and pentagonite, dimorphs of $Ca(VO)(Si_4O_{10})\cdot 4H_2O$.[28] The minerals haradaite, $SrVOSi_2O_6$,[29] and natisite, Li_2VOSiO_4,[30] are also examples of vanadium(IV) silicates but with layered rather than framework structures. Other open-framework transition metal silicates where silicate tetrahedra are connected to transition metal octahedra by sharing corners, for example, $K_3NdSi_6O_{15}\cdot 2H_2O$, have been described, but they have little intracrystalline pore volume.[31,32]

We have recently reported two new open-framework vanadosilicates, VSH-1K and VSH-2Cs,[33] that contain the same structural motifs found in the natural minerals cavansite and pentagonite. We have examined how additional compounds can be formed by different combinations of the same building units and subsequently generalized our synthesis approach. We have obtained, as a result, a large family of open-framework, and in some cases microporous, vanadosilicates with free channel diameters as large as 6.5 Å. We designate the vanadosilicate family *v*anadium *s*ilicate *H*ouston-*n*A (VSH-*n*A), where *n* is the framework type and A represents the nonframework cations. The compounds all contain discrete vanadium centers that are an integral part of the framework and are accessible to molecular and cationic species via the pores. This, together with their high thermal stability, good absorption, and ion-exchange properties, suggests the potential for technological applications in separations and catalysis.[34,35] Further, a large new class of compounds comparable to the zeolite family can be predicted on the basis of the building units found in the VSH-*n*A series.

Experimental Section

Synthesis. The VSH-*n* compounds were synthesized by hydrothermal methods similar to those used in the synthesis of zeolites. Typically, a silica gel was mixed with solutions of $VOSO_4$ and AOH (A = Na, K, Rb, Cs) and subsequently heated at 180−240 °C for 2−14 days under autogenous pressure in a 23-mL Parr hydrothermal reactor. After reactions, the pH values of the supernatant solutions were measured, and the solid products were recovered by vacuum filtration and washed with water to remove any unreacted silica gel and then with methanol.

Crystals or microcrystalline powders of the different VSH-*n*A compounds were recovered, depending on the specific alkali cation. Water contents of the products were determined by thermogravimetric analysis and the V:M:Si ratios by electron microprobe analysis. The crystals of the vanadium silicates have characteristic green-blue or light blue colors and have crystal sizes of 40 to 500 μm. With the exception of VSH-6CsK, -11RbNa, and -12Cs, the VSH-*n*A phases were obtained in high yield as pure phases. VSH-6CsK was obtained in 60% yield together with an unidentified silicate impurity, VSH-11RbNa, and -12Cs as minor phases.

A systematic approach was used to investigate the influence of composition on the reaction products. An example is shown in Figure 1 for compounds prepared using CsOH, $VOSO_4$, and SiO_2 as reactants. The diagram shows the pH values of the solution phases at the end of the reaction for a series of 24 reactions carried out at 220 °C. The diagram indicates the regions where particular phases predominate, in

(27) Rocha, J.; Brandão, P.; Lin, Z.; Anderson, M. W.; Alfredsson, V.; Terasaki, O. *Angew. Chem., Int. Ed. Engl.* **1997**, *36*, 100.
(28) Evans, H. T. *Am. Mineral.* **1973**, *58*, 412.
(29) Takeuchi, Y.; Joswig, W. *Mineral. J. (Jpn.)* **1967**, *5*, 98.
(30) Rangan, K. K.; Piffard, Y.; Joubert, O.; Tournoux, M. *Acta Crystallogr.* **1998**, *C54*, 176.
(31) Haile, S. M.; Wuensch, B. J. *Am. Mineral.* **1997**, *82*, 1141.
(32) Liebau, F. *Structural Chemistry of Silicates: Structure, Bonding and Classification*; Springer-Verlag: Berlin, 1985.
(33) Wang, X.; Liu, L.; Jacobson, A. J. *Angew. Chem., Int. Ed.* **2001**, *40*, 2174.
(34) Venuto, P. B. *Microporous Mater.* **1994**, *2*, 297.
(35) Thomas, J. M. *Angew. Chem., Int. Ed.* **1999**, *38*, 3588.

Table 1. Crystallographic Data for Selected VSH-*n* Phases

name	formula	space group	*a* (Å)	*b* (Å)/*β* (deg)	*c* (Å)	*R*(*F*)	silicate layer
VSH-1K	$K_2(VO)(Si_4O_{10})\cdot H_2O$	*Pbca*	10.258(2)	8.260(2)	12.981(3)	0.055	L1a
VSH-2Cs	$Cs_2(VO)(Si_6O_{14})\cdot 3H_2O$	*Cmca*	17.051(2)	8.6630(9)	12.384(1)	0.042	L5
VSH-3Rb	$Rb_2(VO)_2(Si_6O_{15})\cdot 1.6H_2O$	$Cmc2_1$	15.614(9)	8.360(5)	13.142(8)	0.077	L1b
VSH-3K	$K_2(VO)_2(Si_6O_{15})\cdot 1.6H_2O$	$Pbc2_1$	15.494(2)	8.2673(9)	13.147(2)	0.045	L1b
VSH-4Cs	$Cs_2(VO)(Si_4O_{10})\cdot 2.7H_2O$	$R\bar{3}m$	13.392(2)	13.392(2)	21.568(4)	0.050	L3
VSH-4Rb	$Rb_2(VO)(Si_4O_{10})\cdot 3H_2O$	$R\bar{3}m$	13.2878(8)	13.2878(8)	21.256(2)	0.111	L3
VSH-6CsK	$(Cs,K)_2(VO)(Si_4O_{10})\cdot 3H_2O$	*P*31*c*	13.11(1)	13.11(1)	14.35(2)	0.142[a]	L3
VSH-6Rb	$Rb_2(VO)(Si_4O_{10})\cdot 3H_2O$	$P6_3/mmc$	13.1698(6)	13.1698(6)	14.5054(8)	0.079[a]	L3
VSH-9CsNa	$CsNa(VO)(Si_4O_{10})\cdot 4H_2O$	$R\bar{3}m$	13.5674(7)	13.5674(7)	21.855(2)	0.076	L3
VSH-11RbNa	$(Rb,Na)_2(VO)(Si_4O_{10})\cdot xH_2O$	$R\bar{3}m$	18.2124(7)	18.2124(7)	45.752(2)	0.122	L4a, L4b
VSH-12Cs	$Cs_2(VO)(Si_4O_{10})\cdot xH_2O$	*Pbam*	12.690(3)	14.916(3)	6.984(1)	0.117[a]	L2a
VSH-12LiX	$Li_2(VO)(Si_4O_{10})\cdot xH_2O$	*Pbam*	12.859(3)	14.911(4)	7.078(2)	0.093[b]	L2a
VSH-13Na	$Na_2(VO)(Si_4O_{10})\cdot 3H_2O$	*Imma*	14.409(9)	9.129(6)	10.452(7)	0.059	L2b
VSH-14Na	$Na_2(VO)(Si_4O_{10})\cdot 1.4H_2O$	*C*2/*c*	27.544(4)	8.690(1)/109.6(1)	10.061(2)	0.071	L1a

[a] Superposition stucture models of disorder. [b] Ion-exchanged single crystal.

this case VSH-2Cs, VSH-4Cs, and VSC-1. In this particular example, VSC-1 is another new phase that is not structurally related to the VSH-*n*A compounds and is described elsewhere.[36] Usually some optimization of the conditions is required after the initial synthesis to obtain high-yield, single-phase products.

Ion Exchange. Ion exchange experiments were carried out by stirring powder samples in a large excess of the exchanging ion in aqueous solution (1 M) at 50 °C for several hours. The products were filtered and then washed with deionized water and methanol.

X-ray Crystallography. The structures of the VSH-*n* series were determined from single-crystal X-ray diffraction data. All measurements were made with a Siemens SMART platform diffractometer equipped with a 1K CCD area detector. In a typical experiment, a hemisphere of data (1271 frames at 5-cm detector distance) was collected using a narrow-frame method with scan widths of 0.3° in ω and an exposure time of 20−40 s/frame. The first 50 frames were remeasured at the end of data collection to monitor instrument and crystal stability, and the maximum correction applied to the intensities was <1%. The data were integrated using the Siemens SAINT program,[37] with the intensities corrected for Lorentz factor, polarization, air absorption, and absorption due to variation in the path length through the detector faceplate. The structures were solved by direct methods and refined on F^2 by full-matrix least squares using SHELXTL.[38] The crystallographic data are summarized in Table 1.

The structures of VSH-6CsK and VSH-6Rb are highly disordered, as evidenced by strong diffuse streaking observed with the area detector. A subcell was derived by ignoring the streaking reflections for each of the two phases. Superposition structure models with averaged atom positions of the disordered structures were solved and refined using the subcell. For VSH-12Cs, the structure was solved and refined using the unit cell listed in Table 1. Very weak but sharp superstructure reflections were also observed which indicate an orthorhombic unit cell with $a = 25.378(2)$, $b = 29.831(3)$, and $c = 13.967(1)$ Å. Efforts to solve this superstructure were unsuccessful. The remaining phases, with the exception of VSH-4Rb, have ordered frameworks, and the structure refinements for them were quite straightforward. For VSH-4Rb, electron density peaks in the difference maps indicate a small fraction (∼10%) of stacking disorder of the framework, which was successfully incorporated in the final refinements.

In all the VSH-*n* phases, the extraframework alkali cations and water molecules were found partially or fully disordered. Composition constraints based on the chemical and thermogravimetric analyses were applied in the structure refinements in order to refine relative occupancies of different sites. Discrimination between the alkali cations and water oxygen positions is sometimes ambiguous, particularly when the sites are partially occupied; specific bonding considerations were used to make some assignments.

Characterization. Electron probe microanalysis (EPMA) for chemical compositions was carried out on a JEOL 8600 electron microprobe at 15 keV, 10 μm beam diameter, and 30 nA beam current. For some samples, peaks from alkali metal cations were observed to diminish during the EPMA measurements due to sample instability in the electron beam. Several samples were analyzed by EDX using a JEOL JSM 6400 scanning electron microscope with a Link Analytical EXL spectrometer. Thermogravimetric analysis (TGA) was carried out in a simulated air flow with a heating rate of 5°/min on a TA Instruments Hi-Res 2950 system. Infrared spectra were collected with a Galaxy FTIR 5000 spectrometer using the KBr pellet method. UV−vis−NIR diffuse reflectance spectra were measured with a Cary 500 spectrophotometer on powder samples at room temperature. Magnetic susceptibilities for selected samples were measured using a Quantum Design SQUID magnetometer and an applied field of 5000 G between 4 and 300 K. Nitrogen absorption isotherms were measured using a Quantachrome Nova 2000 instrument. Samples were outgassed by heating under vacuum at 300 °C before the nitrogen absorption measurements.

Results

Synthesis and Characterization. The syntheses and characterization of VSH-1 and VSH-2 were previously reported.[33] The starting materials were fumed silica (Acros Organics, Cab-o-sil M-5 Scintillation grade), $VOSO_4\cdot 3H_2O$ (Aldrich), CsOH (Aldrich), RbOH (Aldrich), KOH (EM Science), and NaOH (EM Science) and were used as received.

VSH-3Rb. Solutions of 2.5 M $VOSO_4\cdot 3H_2O$ (0.96 mL, 2.4 mmol) and 4.24 M RbOH (1.42 mL, 6.0 mmol), together with 0.436 g of a mixture of 5.7 g of fumed silica (1.6 mmol) and 20 mL of H_2O, were heated at 220 °C for 3.75 d. VSH-3Rb: sky blue crystals, yield ∼60%; EPMA, V:Rb:Si = 2.0:1.1:6.6; TGA, ∼0.8 H_2O per V atom; infrared spectrum (cm^{-1}), 471 (s), 531 (m), 591 (m), 690 (w), 714 (w), 792 (m), 912 (w), 986 (sh), 1011 (s), 1060 (s), 1106 (s), 1128 (sh), 1630 (wm), 1654 (m), 2851 (w), 2927 (w), 3265 (w), 3397 (m), 3470 (m), 3566 (sh), 3580 (m).

VSH-3K. Solutions of 2.5 M $VOSO_4\cdot 3H_2O$ (0.96 mL, 2.4 mmol) and 4.24 M KOH (0.94 mL, 4 mmol), together with 0.982 g of a mixture of 5.7 g of fumed silica (3.6 mmol) and 20 mL of H_2O, were heated at 220 °C for 3.75 d. VSH-3K: sky-blue crystals, yield ∼70%; EPMA, V:Si = 1.0:3.6; TGA, ∼0.8 H_2O per V atom; infrared spectrum (cm^{-1}), 415 (m), 468

(36) Wang, X.; Liu, L.; Zhang, G.; Jacobson, A. J. *Chem. Commun.* **2001**, 2472.
(37) SAINT, *Program for Data Extraction and Reduction*; Siemens Analytical X-ray Instruments, Madison, WI, 1994−1996.
(38) SHELXTL (*version 5.0*) *Reference Manual*; Siemens Industrial Automation, Analytical Instrumentation, Madison, WI, 1995.

(s), 524 (m), 593 (m), 698 (w), 714 (w), 793 (m), 806 (sh), 918 (m), 981 (s), 1017 (s), 1060 (s), 1102 (s), 1628 (wm), 1665 (m), 3280 (m), 3377 (m), 3458 (m), 3532 (m), 3578 (m).

VSH-4Cs. Solutions of 2.5 M $VOSO_4 \cdot 3H_2O$ (0.32 mL, 0.8 mmol) and 4.24 M CsOH (1.42 mL, 6 mmol), together with 0.873 g of a mixture of 5.7 g of fumed silica (3.2 mmol) and 20 mL of H_2O, were heated at 220 °C for 3.75 d. VSH-4Cs: pale blue green crystals, yield ~95%; EPMA, V:Cs:Si = 1.0:1.8:4.5; TGA, 2.7 H_2O per V atom; infrared spectrum (cm^{-1}), 412 (m), 517 (m), 537 (sh), 576 (m), 645 (w), 675 (m), 773 (w), 977 (s), 1000 (s), 1099 (sh), 1171 (m), 1638 (m), 3429 (br), 3578 (sh).

VSH-4Rb. Solutions of 1 M $VOSO_4 \cdot 3H_2O$ (0.5 mL, 0.5 mmol) and 8.5 M RbOH (0.34 mL, 2.9 mmol), together with 0.62 g of a mixture of 5.5 g of fumed silica (2.2 mmol) and 20 mL of H_2O, 0.66 mL of H_2O, and 1 mL of ethylene glycol, were heated at 200 °C for 3.6 d. VSH-4Rb: blue-green crystals, yield ~95%; EPMA, V:Rb:Si = 1.0:1.8:4.3; TGA, ~3.0 H_2O per V; infrared spectrum (cm^{-1}), 413 (m), 517 (m), 537 (sh), 580 (m), 653 (w), 683 (m), 783 (w), 980 (s), 1003 (s), 1043 (sh), 1167 (m), 1643 (m), 3467 (br), 3596 (sh).

VSH-6CsK. Solutions of 2.5 M $VOSO_4 \cdot 3H_2O$ (0.4 mL, 1 mmol), 4.24 M KOH (0.59 mL, 2.5 mmol), and 4.24 M CsOH (0.59 mL, 2.5 mmol), together with 1.09 g of a mixture of 5.7 g of fumed silica (4 mmol) and 20 mL of H_2O, were heated at 230 °C for 3.75 d. VSH-6CsK: pale blue green crystals, yield ~60% plus unidentified impurity; EPMA, V:K:Cs:Si = 2.0:1.3:1.6:8.3; TGA, ~2.4 H_2O per V atom; infrared spectrum (cm^{-1}), 408 (m), 425 (sh), 494 (sh), 514 (sh), 537 (m), 573 (m), 606 (m), 649 (w), 698 (m), 777 (m), 797 (m), 977 (s), 1017 (s), 1063 (sh), 1155 (s), 1651 (m), 3249 (sh), 3470 (br), 3566 (br), 3613 (br).

VSH-6Rb. Solutions of 2.5 M $VOSO_4 \cdot 3H_2O$ (0.64 mL, 1.6 mmol) and 4.24 M RbOH (1.42 mL, 6 mmol), together with 0.654 g of a mixture of 5.7 g of fumed silica (2.4 mmol) and 20 mL of H_2O, were heated at 220 °C for 3.75 d. VSH-6Rb: blue-green crystals, yield ~90%; TGA, ~3 H_2O per V atom; infrared spectrum (cm^{-1}), 409 (m), 501 (sh), 520 (m), 540 (sh), 573 (m), 606 (m), 652 (w), 701 (m), 774(sh), 790 (w), 971 (s), 1010 (s), 1060 (sh), 1165 (s), 1635 (sh), 1651 (m), 3241 (sh), 3474 (br), 3543 (br), 3613 (br).

VSH-9CsNa. Solutions of 2.5 M $VOSO_4 \cdot 3H_2O$ (0.32 mL, 0.8 mmol), 4.24 M NaOH (0.71 mL, 3 mmol) and 0.71 mL of 4.24 M CsOH (3 mmol), together with 0.873 g of a mixture of 5.7 g of fumed silica (3.2 mmol) and 20 mL of H_2O, were heated at 230 °C for 3.75 d. VSH-CsNa: blue green crystals, yield ~90%; semiquantitative EDX analysis gave atomic ratios V:Na:Cs:Si = 1.0:0.5:1.0:4.9; TGA, ~4 H_2O per V atom; infrared spectrum (cm^{-1}), 411 (m), 472 (w), 546 (m), 583 (m), 630 (w), 676 (w, sh), 704 (m), 773 (w), 783 (w), 987 (s), 1015 (s), 1122 (m), 1145 (sh), 1642 (m), 3251 (sh), 3503 (br).

VSH-11RbNa. Solutions of 2.5 M $VOSO_4 \cdot 3H_2O$ (0.64 mL, 1.6 mmol), 4.24 M NaOH (0.71 mL, 3 mmol), and 4.24 M RbOH (0.71 mL, 3 mmol), together with 0.654 g of a mixture of 5.7 g of fumed silica (2.4 mmol) and 20 mL of H_2O, were heated at 230 °C for 3.75 d. VSH-11RbNa: pale blue crystals, minor phase; infrared spectrum (cm^{-1}), 411 (ms), 523 (m), 542 (m), 574 (m), 607 (m), 699 (m), 769 (sh), 792 (w), 973 (s), 1015 (s), 1062 (sh), 1159 (s), 1647 (m), 3240 (sh), 3497 (br), 3601(sh).

VSH-12Cs. Solutions of 2.5 M $VOSO_4 \cdot 3H_2O$ (0.32 mL, 0.8 mmol) and 4.24 M CsOH (1.42 mL, 6 mmol), together with 0.2 g of Mo metal and 0.874 g of a mixture of 5.7 g of fumed silica (3.2 mmol) and 20 mL of H_2O, were heated at 220 °C for 5 d and cooled in an oven over a period of one week. VSH-12Cs: blue green crystals, minor phase; EPMA, V:Cs:Si:Mo = 1.0:1.2:4.5:0.0.

VSH-13Na. Fumed silica (0.188 g, 3.125 mmol) was dissolved in 4.24 M aqueous NaOH (1.35 mL, 5.7 mmol). To this solution was added a 2.5 M solution of $VOSO_4$ (0.6 mL, 1.5 mmol) and 0.2 mL of H_2O. The combined solution was heated at 225 °C for 6 d. VSH-13Na: blue crystals, yield ~90%; TGA, 3.3 H_2O per V atom; infrared spectrum (cm^{-1}), 444 (s), 495-(w), 523 (w), 537 (w), 583 (m), 695 (s), 788 (w), 964 (s), 1001 (s), 1034 (sh), 1136 (s), 1624 (m), 1689 (mw), 3470 (m), 3514 (m), 3607(s).

VSH-14Na. Fumed silica (0.188 g, 3.1 mmol) was dissolved in 4.24 M aqueous NaOH (1.35 mL, 5.72 mmol). To this solution was added a 2.5 M solution of $VOSO_4$ (0.56 mL, 1.4 mmol). The combined solution was heated at 220 °C for 7 d. VSH-14Na: blue crystals, yield ~90%; TGA, 1.4 H_2O per V atom; infrared spectrum (cm^{-1}), 458 (s), 514 (m), 570 (m), 596 (sh), 639 (m), 688 (w), 767 (w), 787 (sh), 931 (s), 958 (s), 984 (s), 1023 (s), 1060 (sh), 1089 (s), 1122 (sh), 1175(s), 1631 (m), 3238 (sh), 3428 (br), 3509 (br), 3629 (sh).

Structures. The VSH-*n*A structures are all based on the same structural principle whereby silicate layers are bridged by VO^{2+} ions to form frameworks; water molecules and nonframework A^+ cations fill the intracrystalline pore space. Except for VSH-2Cs (Table 1), the VSH-*n*A structures contain single silicate layers with the composition $Si_2O_5^{2-}$ ($SiO_{3/2}O_{1/1}^-$). In the layers, each SiO_4 tetrahedron shares three oxygen atoms with other tetrahedra; the fourth oxygen atom is terminal. Three-connected plane nets can be used to describe the possible arrangements of the tetrahedra within each single silicate layer.[39] Rather than discussing the structures of the individual compounds in a serial fashion, we use this description to classify and compare the structures that we have found to date. The details of all of the structures are provided in the Supporting Information. The different silicate layers found to date in the VSH-*n*A phases and their net designations are shown in Figure 2. The layer type of each VSH-*n*A compound is given in Table 1. The silicate layers in the natural minerals pentagonite and cavansite are closely similar to L1a and L2b, respectively.

Silicate layers with different orientations of the SiO_4 tetrahedra (either up or down) can correspond to the same three-connected plane net. Thus, the layers of VSH-1, VSH-3, VSH-14, and pentagonite differ from each other in the orientation of the terminal oxygen atoms, but all correspond to the plane net 6^3. A single type of silicate layer is found in all structures except in the structure of VSH-11, which has two different silicate layers (designated L4a and L4b), both corresponding to the plane net (4.6.8)(4.8.12). The layers L4a and L4b are closely related because both can be constructed with the same 12-tetrahedra unit shown in Figure 3, containing a 6-ring and three 4-rings of tetrahedra. In L4a, the terminal oxygen atoms of the 6-ring and those of the other six tetrahedra point in opposite directions (Figure 3a), whereas in layer L4b the terminal oxygen atoms of all 12 tetrahedra point in the same direction (Figure 3b). For

(39) O'Keeffe, M.; Hyde, B. G. *Proc. R. Soc. A* **1980**, *295*, 553.

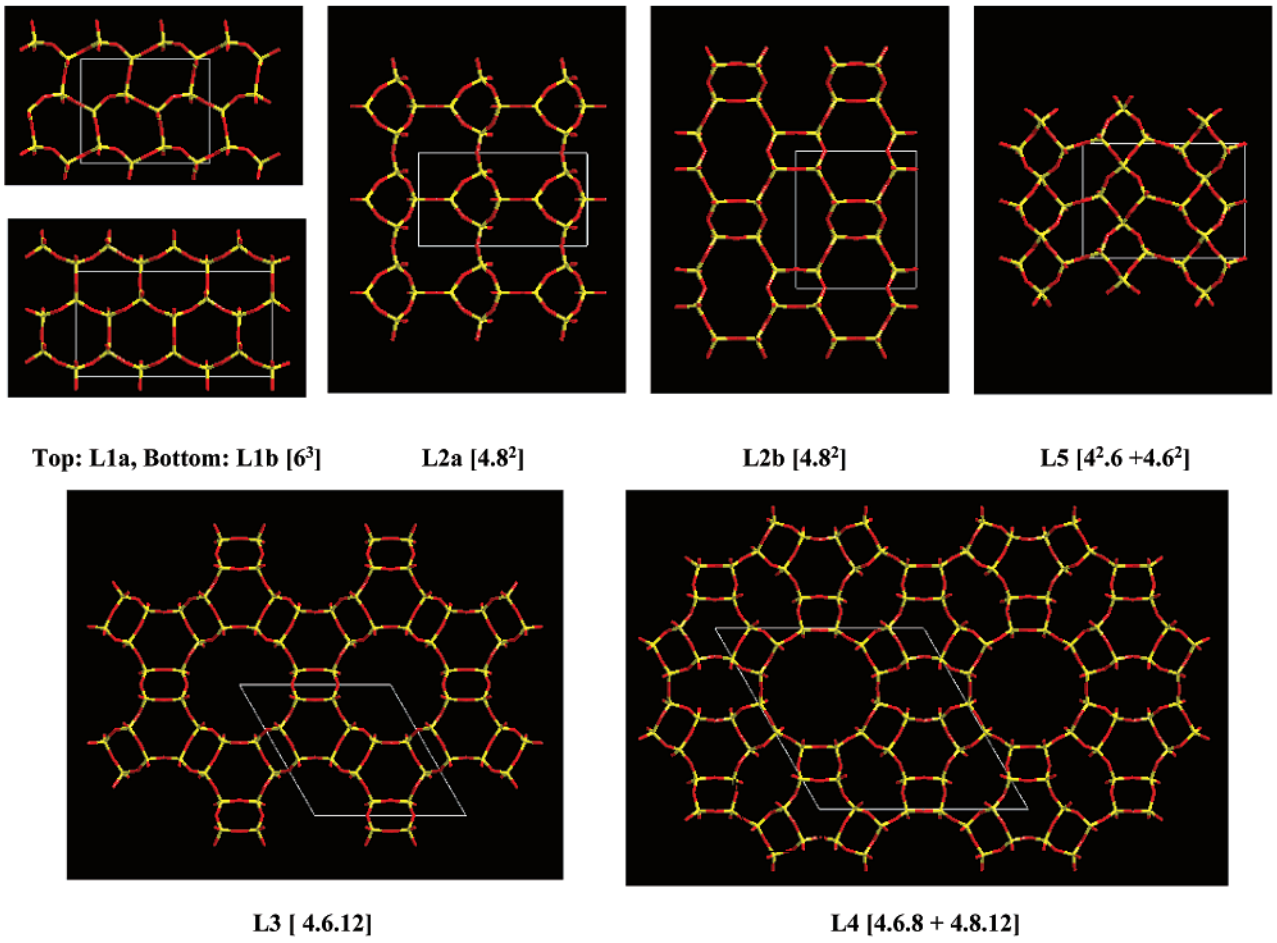

Figure 2. Silicate single layers found in the VSH-*n* phases. Silicon and oxygen atom positions are shown in yellow and red, respectively. Symbols for the 3-connected plane net corresponding to the specific layers are given in square brackets.

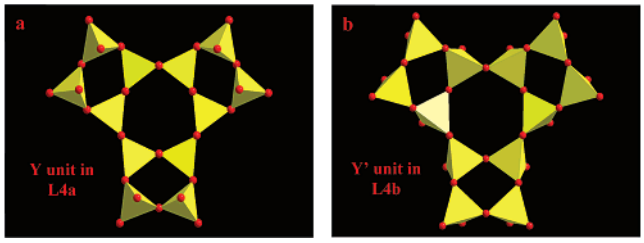

Figure 3. Y (a) and Y′ (b) arrangements of SiO_4 tetrahedra.

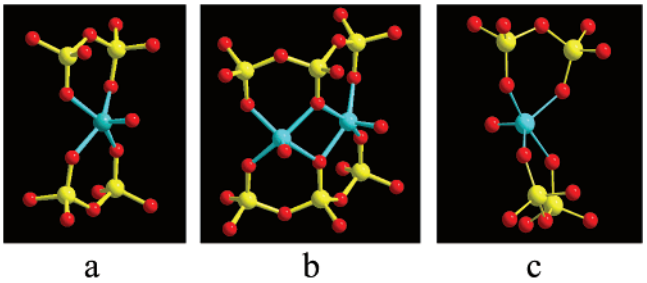

Figure 4. Interlayer VO_5 pyramids and their relations to the silicate tetrahedra: (a) VO_5 pyramidal monomer, (b) V_2O_8 pyramidal dimer, and (c) trigonal bipyramid. Yellow, blue, and red spheres represent silicon, vanadium, and oxygen atoms, respectively.

convenience, we designate these two units as Y and Y′, respectively. Layer L3 can also be formed by a different arrangement of Y building units.

In the VSH-*n* family, VO_5 tetragonal pyramids or (H_2O)-VO_5 distorted octahedra interconnect the silicate layers to form framework structures with open channels. Charge-balancing alkali metal cations and water molecules are found within the channels. The VO_5 pyramids share oxygen atoms with SiO_4 tetrahedra, as shown in Figure 4, and form single or double bridges.

Typically, the square pyramids are disordered over two possible orientations. In the case of single bridges, the silicate layers are required to have terminal oxygen atoms pointing up and down in pairs, while the double bridges in VSH-3K and VSK-3Rb require groups of three in the same orientation. VSH-14 is an exception to the general rule in that equal numbers of V(IV) cations have square pyramidal and trigonal bipyramidal coordination geometry (Figure 4c). Many zeolite structures can be described in terms of stacking of layers, an approach that is particularly useful for understanding relationships between different structures and disorder.[40] The VSH-*n* phases can also be described in this way. VSH-4 has an ordered stacking arrangement of the layer L3. Each layer is shifted by $(a-b)/3$ relative to its neighbors, and therefore the stacking sequence is *ABC* (Figure 5). This stacking sequence results in the centrosymmetric cage *C1* shown in Figure 6a, in which two 6-rings in

(40) Treacy, M. M. J.; Vaughan, D. E. W.; Strohmaier, K. G.; Newsam, J. M. *Proc. R. Soc. London A* **1996**, *452*, 813.

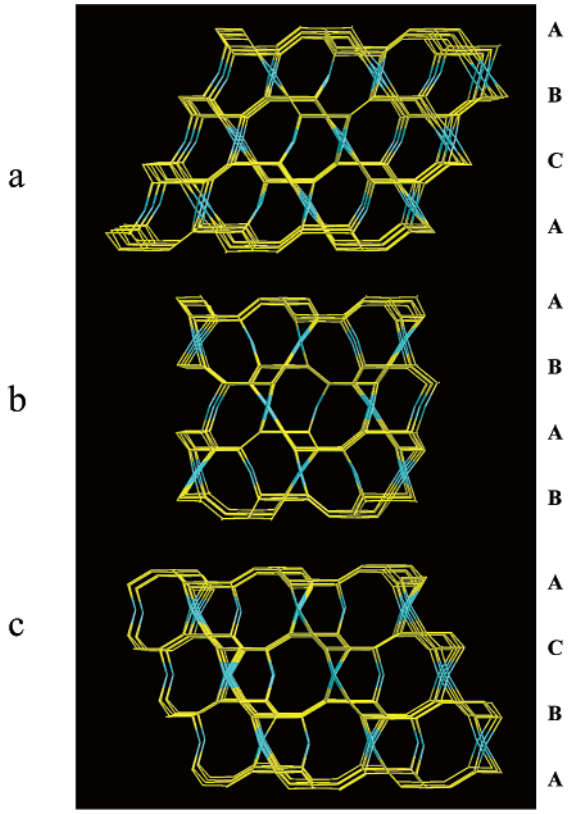

Figure 5. Frameworks of VSH-4 (a), VSH-6 (b), and VSH-9 (c) formed by different stacking of the silicate layer L3. The stacking sequences are *ABC*, *AB*, and *ACB*, respectively. Yellow represents silicon sites and blue vanadium sites. The bridging oxygen atoms are omitted.

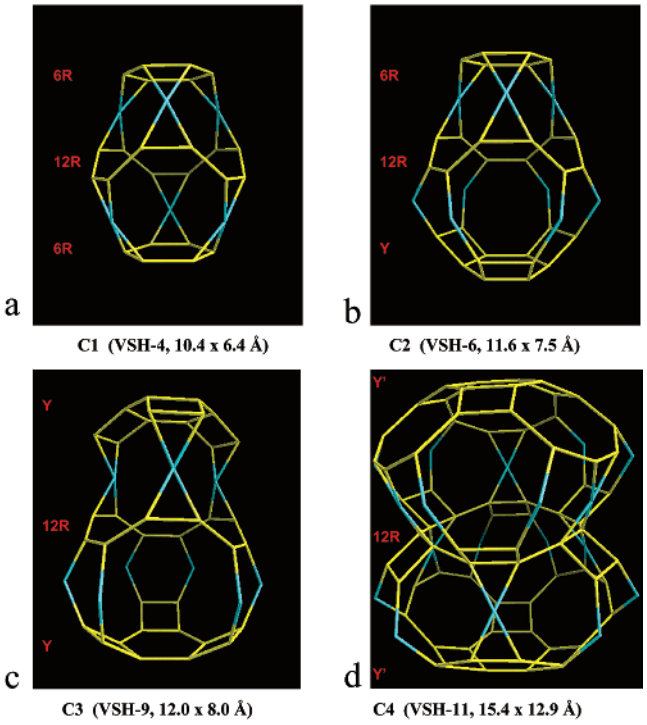

Figure 6. Cages in (a) VSH-4 (*C1*), (b) VSH-6 (*C2*), (c) VSH-9 (*C3*), and (d) VSH-11 (*C4*).

the same orientation are found on either side of a puckered 12-ring. The six 8-ring windows in *C1* are lined up in the structure to form channels along [100] with an aperture of 3.5 Å. The cage itself has a free inner space of 6.4 × 6.4 × 10.3 Å.

An ordered *AB* stacking of the L3 layer requires a nonequivalent arrangement of the interlayer pyramids on the two sides of the layer and has not been observed. The nonequivalency of the pyramid arrangement can be avoided, however, in $\overline{AB}$ stacking, where the neighboring layers are related by a glide plane with a translation $(a-b)/3$ (Figure 5b). The structure of VSH-6 was refined with an ordered $\overline{AB}$ stacking model, although the crystal showed strong diffuse reflections indicating some stacking disorder. In $\overline{AB}$ stacking, the 12-rings of the layer L3 are connected to a 6-ring on one side and the unit shown in Figure 3a (Y) on the other side, giving rise to a noncentrosymmetric cage (cage *C2*, Figure 6b) with a larger internal volume than cage *C1* of VSH-4. The VSH-6 framework is polar with a single orientation of the calabash-shaped *C2* cages.

An ordered *ACB* stacking of the L3 layer is observed in VSH-9. Note that the stacking sequences *ABC* and *ACB* are not equivalent because the layers are nonplanar. Different interlayer arrangements of the bridging VO^{2+} and different channels in the structure are a consequence. An even larger noncentrosymmetric cage (cage *C3*, Figure 6c) formed by connecting each 12-ring to Y units on either side is found in this structure. The cage *C3* has a free inner space 8.0 × 8.0 × 12.0 Å and has 10-ring windows. The VSH-9 framework is traversed by [100] zigzag channel systems with an aperture outlined by 10-rings. In principle, the layers L3 can also be stacked in *AA* or $\overline{AA}$ sequences and linked by VO_5 pyramids in similar ways to VSH-4 and VSH-9, respectively. The stacking sequences *AA* or $\overline{AA}$ lead to framework structures with one-dimensional 12-ring channel systems along the stacking direction and 8-ring or 10-ring channels parallel to the layers, respectively. We have not yet observed these stacking sequences.

In VSH-11, two different types of silicate single layers, L4a and L4b, are stacked alternately. The stacking sequence can be considered as an ordered *ABC* stacking of a two-layer unit [L4aL4b] that is shifted by $(a-b)/3$ relative to its neighbors. The positional relation of the layers L4a and L4b within the unit may be considered as AC if the difference in orientations of terminal oxygen atoms is ignored. The Y′ unit of the layer L4b can only be linked to pyramids on one side, which gives the possibility of forming a large cavity on the other side. The 12-rings of layer L4a are capped by the Y′ units from both sides to form large dumb-bell-like cages *C4* (Figure 6d) that have a free volume of 15.4 × 12.9 × 12.9 Å. The 12-rings of layer L4b have 6-rings on both sides, forming smaller cages that are similar to cage *C1*. VSH-11 has channels along [100] defined by 8- and 7-rings, respectively.

The silicate layers of VSH-12 and VSH-13 both correspond to the plane net 4.8^2 but have different orientations of tetrahedra (Figure 2, L2a, L2b). In the structure of VSH-13, the silicate layers are flat and contain crankshaft chains of tetrahedra that have terminal corners on the same side. A mirror plane relates neighboring layers. Between the layers, octahedral V═O—V═O chains are formed in which the oxygen atom of the V═O group makes a long bond (3.0 Å) trans to the V═O group of a neighboring VO_5 unit. Straight 10-ring channel systems with an aperture 6.5 × 6.5 Å are formed that are parallel to the octahedral chains (Figure 7). The framework of VSH-13 can also be described as consisting of one-dimensional $[VOSi_4O_{12}]$ columns. Each column contains an octahedral chain surrounded

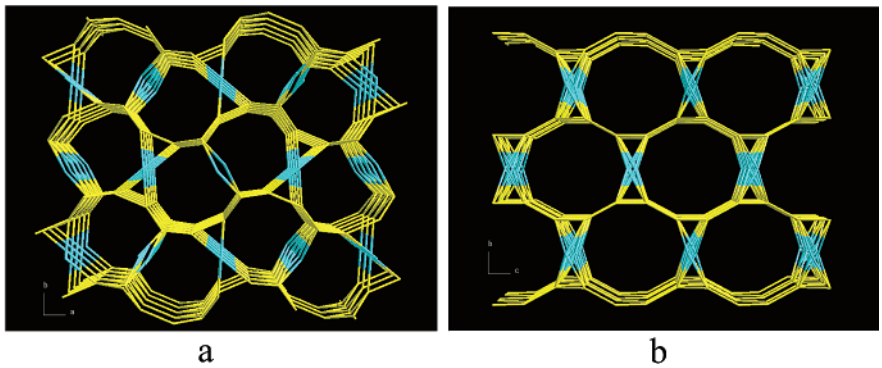

Figure 7. Views of the frameworks of VSH-12 (a) and VSH-13 (b) along their 9-ring and 10-ring channel axes, respectively.

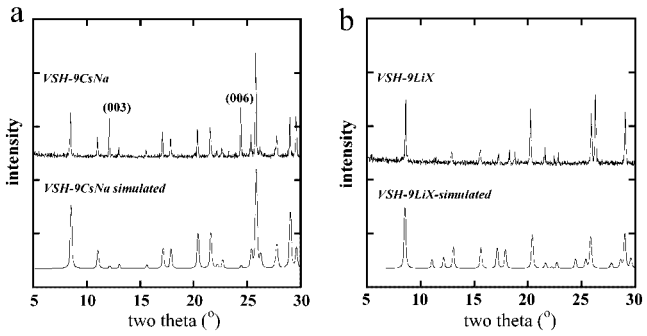

Figure 8. Observed and simulated X-ray powder diffraction data for (a) VSH-9CaNa and (b)VSH-LiX after ion exchange.

by two zigzag silicate chains. Similar columnar units are found in the structure of ETS-10. The structure of VSH-12 contains silicate layers which correspond to an undulating 4.8^2 net, and the framework contains one-dimensional channels defined by 9-rings (Figure 7). Similar 9-ring channels are found in the zincosilicates VPI-7 and RUB-17, where 4.8^2 zincosilicate layers are bridged by SiO_4 tetrahedra.[41,42]

Ion Exchange. While we have not yet made a detailed and systematic study of ion exchange of the extraframework cations, we have demonstrated that, for several members of the VSH-*n* family, exchange by other alkali cations such as Li^+ occurs easily. For example, VSH-9CsNa powder was heated and stirred in 30 mL of a 1 M $LiClO_4$ solution at 50 °C for 3, 15, or 40 h and then washed with deionized water and methanol. After ion exchange, the sample was characterized by X-ray powder diffraction. The measured diffraction patterns before and after the ion exchange reaction were compared with the simulated patterns. The simulated patterns were calculated from the single-crystal structure data and by replacing one cesium atom and the Na atoms with Li for the exchange sample. The diffraction patterns are shown in Figure 8. The agreement between the observed and simulated patterns is very good, though the data for the original sample show significant enhancement of the (003) and (006) intensities due to preferred orientation effects.

Elemental analysis of VSH-9LiX after the lithium ion exchange gave 2.48% Li, 11.76% Cs, 0.034% Na, 11.05% V, and 25.18% Si, which can be compared with calculated values for $CsNa(VO)(Si_4O_{10})\cdot 3H_2O$ (24.2% Cs, 4.19% Na, 9.27% V, 20.5% Si) and complete exchange $Li_2(VO)(Si_4O_{10})\cdot 3H_2O$ (3.4% Li, 12.5% V, 27.6% Si). The results show almost complete removal of the Na^+ and partial exchange of Cs^+.

VSH-4Rb was ion exchanged in 1 M $LiClO_4$ solution in the same way. After ion exchange, the X-ray powder diffraction pattern is close to the pattern simulated from the structure data by replacing Rb with Li. Elemental analysis after the lithium ion exchange gave 2.2% Li, 7.12% Rb, 10.67% V, and 25.91% Si. The atomic ratios of Li:Rb:V are 1.52:0.4:1 after the ion exchange compared to Rb:V = 2:1 before. The ion exchange removal of Rb cations increases the micropore volume, and consequently the exchange sample contains more water molecules. The sample weight loss determined by thermogravimetric analysis was 17.22%, corresponding to 4 H_2O after ion exchange compared to 9.48% or 3 H_2O per formula unit before exchange.

A prismatic single crystal of VSH-12Cs with approximate dimensions 0.25 × 0.16 × 0.10 mm was immersed in a reservoir of $LiClO_4$ solution (1 M, 20 mL) for 30 days at room temperature without stirring. The crystal was then separated from the solution and found to be cracked into several pieces. One piece with size ~0.05 × 0.06 × 0.08 mm was found suitable for single-crystal X-ray diffraction and was used for data collection. Structure refinements indicate that all strong electron density peaks corresponding to extraframework Cs atoms disappeared, while the framework shows no substantial change after the ion exchange. The results are given in Table 1.

Thermal Stability and Nitrogen Absorption. Thermogravimetric analysis shows that the VSH-*n* series fall into two distinct group of compounds with respect to their water desorption behavior. In one group (VSH-1K, -3K, -3Rb, -13Na, and -14Na), the water desorption occurs above 100 °C in a distinct step(s), indicative of small channel systems with discrete coordinated water molecules. Data for VSH-13Na, for example, show two distinct weight changes on both heating and cooling, and water absorption and desorption is reversible with respect to the amount gained and lost, but some hysteresis is observed under the experimental conditions used (2 °C min^{-1}). The other members of the VSH-*n* series show behavior that is typical for zeolites, namely that a continuous loss of water is observed from the initial temperature. The water desorption data are paralleled in the infrared data by the observation of increasingly sharp bands in the 4000−2500 cm^{-1} region as a consequence of well-defined cation coordination and hydrogen bonds.

Preliminary studies show that the VSH-*n* frameworks have "zeolitic" properties that are consistent with their structures. As examples, VSH-4 and VSH-9 show excellent thermal stabilities (to 500 °C) and reversible dehydration−rehydration properties, as confirmed by X-ray powder diffraction and thermogravimetric analysis. As discussed above, enhanced water absorption

(41) Röhrig, C.; Gies, H.; Marler, B. *Zeolites* **1994**,*14*, 498.
(42) Röhrig, C.; Gies, H. *Angew. Chem., Int. Ed. Engl.* **1995**, *34*, 63.

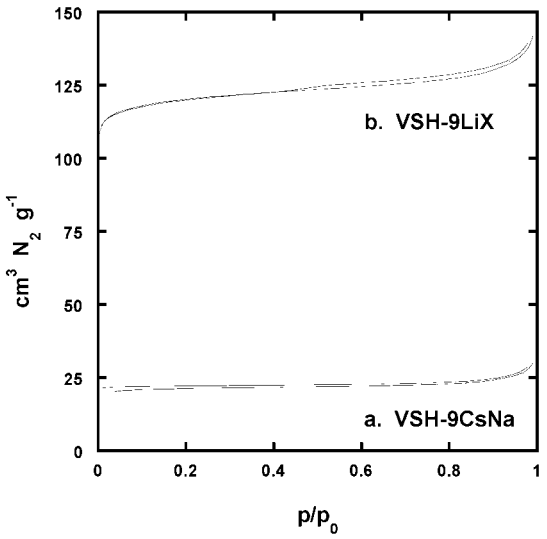

Figure 9. Nitrogen absorption isotherms for (a) $CsNa(VO)(Si_4O_{10})\cdot 3H_2O$ (VSH-9CsNa) and (b) lithium-exchanged (VSH-9LiX).

capabilities were observed after exchange of Li^+ for the larger alkali cations. The nitrogen absorption isotherms for VSH-9CsNa and VSH-9LiX are shown in Figure 9. For both compositions, type 1 absorption is observed, indicative of true microporosity. The partial removal of Cs by ion exchange results in a significant increase in the volume of nitrogen absorbed from 25 to 125 $mL^3\ g^{-1}$.

Spectroscopy. The infrared spectra show the expected features for polymerized silicate tetrahedra, $V{=}O^{2+}$ groups, and intracrystalline water. In zeolites, the infrared features are usually grouped into the internal stretching modes of the SiO_4 tetrahedra and vibrations that are sensitive to the specific tetrahedra linkages. The strongest modes due to SiO_4 asymmetric stretching occur in the frequency range 950−1250 cm^{-1}. The internal symmetric stretching modes are observed between 650 and 720 cm^{-1}, while the more intense Si−O−Si bending modes are found at 420−500 cm^{-1}.[1] The vanadyl stretching vibrations are observed typically at 1000−985 cm^{-1}, though lower values are observed when an additional ligand is coordinated trans to V═O. An additional band is present in VSH-3 at 912 (-Rb) and 918 cm^{-1} (-K) due to the V_2O_8 dimer. VSH-14 has extra bands at 931 and 958 cm^{-1} that may arise from the presence in the structure of two vanadium atoms with different coordination environments. The infrared spectra are compared in Figure 10. The spectra are very similar for VSH-4Rb, -9CsNa, and -6Rb, which all contain the same L3 silicate sheet. In contrast, the spectra for VSH-6Rb, -11RbNa, -14Na, and -13Na, which all contain different silicate layers, have significant differences in both position and intensities of the bands in the region below 650 cm^{-1}, where the frequencies are expected to be sensitive to the type and arrangement of the secondary units in the structure.

It is also apparent in Figure 10 that the H_2O bending mode at 1650 cm^{-1} becomes sharper and eventually splits in the spectrum of VSH-14Na. The symmetric and asymmetric stretching modes in the range 2850−3860 cm^{-1} show parallel behavior with well-defined structure in the cases of VSH-13Na, -14Na, and -3K, where the water molecule coordination environments over multiple sites are well defined. In the larger pore structures, the nonframework cations and water molecules

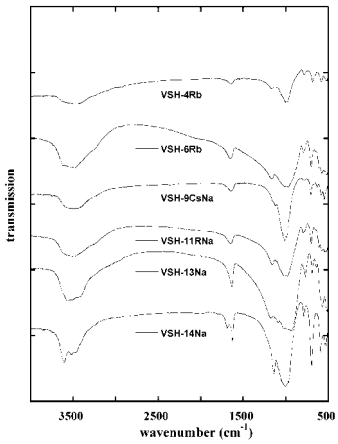

Figure 10. Infrared spectra for VSH-4Rb, -6Rb, -9CsNa, -11RbNa, -14Na, and -13Na containing the silicate layers L3, L3, L3, (L4a, L4b), L1c, and L2b.

are disordered over many positions, and the corresponding spectra are broad.

The diffuse reflectance spectra for VSH-3, -4, and -9 show three absorption bands at 857, 887, 849 nm, 603, 596, 615 nm, and 390, 443, and 435 nm, respectively for the three compounds. The observed absorption bands are assigned to the transitions $d_{yz},d_{xz} \rightarrow d_{xy}$,$d_{x^2-y^2} \rightarrow d_{xy}$ and $d_{z^2} \rightarrow d_{xy}$ by analogy with data for the vanadium hydrogen phosphates that contain either VO_5 square pyramids ($VOHPO_4\cdot 4H_2O$) or V_2O_8 dimers ($VOHPO_4\cdot 0.5H_2O$).[43]

Magnetic Behavior. Magnetic susceptibilities for selected samples were measured using a SQUID magnetometer and an applied field of 5000 G. The VSH-*n* compounds with single bridging VO_5 units show Curie−Weiss behavior with very small Weiss Θ temperatures, as expected from the structural data. The effective moments are close to the value predicted for isolated $V^{4+}(d^1)$ ions. When two bridging units are present, as in VSH-3, the susceptibility data show the presence of weak pairwise antiferromagnetic interactions below ∼10 K.

Summary and Discussion

A series of alkali-metal-containing vanadosilicates has been synthesized under mild hydrothermal conditions. With the exception of VSH-2, the members of the VSH-*n* series have structures that can be derived by connecting three connected sheets of silicate tetrahedra with square pyramidal VO_5 units. The structures that result range from open-framework structures with well-defined nonframework cation and water molecule positions to microporous structures with disordered nonframework species and zeolitic properties.

The VSH-*n* compounds reported here can be classified as a specific group of phyllosilicates and are closely related to the clay minerals sepiolite and palygorskite, in which silicate single layers are linked by interlayer MgO_6 octahedral stripes. The crystal chemistry of hydrous layered silicates has been thoroughly discussed by Liebau.[32] For hydrous silicates containing Si_2O_5 single layers and interlayer metal-centered octahedral units, Liebau concluded that the contour of the silicate layer correlates with the size of interlayer metal cations that are directly bonded to the terminal oxygen atoms of the layer. As

(43) Amorós, P.; Ibáñez, R.; Martinez-Tamayo, E.; Beltrán-Porter, A.; Beltrán-Porter, D. *Mater. Res. Bull.* **1989**, *24*, 1347.

the metal size increases, the silicate layers tend to fold, and areas where tetrahedra have the same orientation (i.e., terminal oxygen atoms on the same side of the layer) decrease. The same trend is observed in the VSH-*n* structures, where the bridging cations are all V^{4+}, as the size of the nonframework alkali cation increases. For instance, the 4.8^2 layers of VSH-13Na are flat, while those of VSH-12Cs are folded (Figure 7). VSH-11RbNa has Y′ units with 12 tetrahedra having the same orientation, while in the layer L3 present in VSH-4Rb, -Cs, VSH-6Rb, -CsK, and VSH-9CsNa, only the tetrahedra in the six-rings have the same orientation. We also note that phases with dense Si_2O_5 layers have a high negative charge density that requires a high interlayer cation density, thus leaving less space for water molecules. For example, VSH-1K, VSH-3K, -Rb, and VSH-14Na all have layers with only six rings and are relatively less hydrated.

Some of the silicate layers in the VSH-*n* compounds are equivalent to the layered building units in typical zeolite structures. The corresponding zeolite tetrahedral frameworks are derived by replacing each VO_5 pyramid with two bridging oxygen atoms. For example, this substitution transforms the frameworks of cavansite and of VSH-13 into the framework of the zeolite gismondine, and the frameworks of VSH-4 and VSH-9 are related to the sodalite and chabazite frameworks, respectively. Such structural relations are interesting because useful precursors to high silica zeolites may be prepared by chemically exfoliating the VSH-*n* compounds.

The VSH-*n* phases formed at high pH (11−13) are dominated by structures with Si_2O_5 single layers connected by VO_5 interlayer pyramids. Under more acidic conditions, condensation of both the silicate layer or/and the interlayer pyramids tends to increase. VSH-2 is an example of the former, where one-third of the tetrahedra in the silicate layer are four-connected. VSH-3 is an example of the latter, where the Si_2O_5 layers are cross-linked by edge-sharing pyramidal dimers (Figure 3). The $V_2O_8 \cdot {}^1/_2H_2O$ dimer structure present in VSH-3Rb is similar to the dimer in the structure of $VO(HPO_4) \cdot {}^1/_2H_2O$.[44] The basal planes of the two square pyramids that share an edge are tilted at average angles of 126° and 117° for the silicate and phosphate, respectively. The smaller tilt angle in the phosphate corresponds to a shorter $V-OH_2$ bond distance (2.35 Å) compared to that in the silicate (2.67 Å); the V═O bond lengths are similar (1.57, 1.60 Å).

In general, the VSH-*n* phases are described by the formula $A_r[(VO)_s(Si_2O_5)_p(SiO_2)_q] \cdot tH_2O$, where A represents the extraframework ions. While increasing $s/(p + q)$ tends to decrease the porosity of the framework, increasing the q/p ratio will have the opposite effect when only single silicate layers are present. In particular, increasing the q/p ratio will lower the charge density of the framework and thus favor incorporation of large organic species into the structure. Organic cations and molecules have been widely used in zeolite syntheses and in mixed octahedral tetrahedral frameworks as structure-directing templates to produce large pores. We are currently investigating this possibility.

The VSH-*n* phases reported here are most likely the first examples of a large family of open-framework vanadium silicates based on well-defined interconnections between silicate tetrahedra and vanadium oxygen square pyramids. The diversity may be further expanded by substitution of the vanadyl groups with other components such as $[ZrF_2]^{2+}$, $[NbOF]^{2+}$, and UO_2^{2+} recently found to link germanate chains and silicate layers into framework structures.[23,45,46]

Acknowledgment. This work was supported by the National Science Foundation under Grant DMR-0120463 and by the Robert A. Welch Foundation. The work made use of MRSEC Shared Experimental Facilities supported by the National Science Foundation under Award No. DMR-9632667.

Supporting Information Available: Six additional figures and vertex symbols for the VSH-*n* frameworks (PDF); X-ray crystallographic data for the structure determinations of the VSH-*n*A compounds except VSH-1 and -2 (CIF). This material is available free of charge via the Internet at http://pubs.acs.org.

JA020354L

(44) Leonowicz, M. E.; Johnson, J. W.; Brody, J. F.; Shannon, H. F., Jr.; Newsam, J. M. *J. Solid State Chem.* **1985**, *56*, 370.
(45) Francis, R. J.; Jacobson, A. J. *Angew. Chem., Int. Ed.* **2001**, *40*, 2879.
(46) Wang, X.; Huang, J.; Liu, L.; Jacobson, A. J. *J. Mater. Chem.* **2002**, *12*, 406.